INTERNATIONAL JOURNAL FOR NUMERICAL METHODS IN ENGINEERING
Int. J. Numer. Meth. Engng 2001; **52**:1165–1188 (DOI: 10.1002/nme.253)

Microplane finite element analysis of tube-squash test of concrete with shear angles up to 70°

Michele Brocca and Zdeněk P. Bažant*,†

Northwestern University, Evanston, IL 60208-3109, U.S.A.

SUMMARY

Finite element analysis of the response of concrete structures to impact events such as missile penetration, explosive driving of anchors, blast, ground shock or seismic loading, requires knowledge of the stress–strain relations for concrete for finite strain at high pressures. A novel type of material test achieving very large shear angles of concrete at very large pressures, called the tube-squash test, can be used to calibrate a concrete model taking into account plastic deformation at extreme pressures. A finite element analysis of such a test is performed by using a finite strain generalization of microplane models for concrete and steel. The results obtained are in good agreement with those previously obtained with a simplified method of analysis. Thus, they provide a validation of the microplane model, which is shown to be capable of reproducing the response of concrete not only for small strains at small pressures, which is predominantly brittle, but also for high pressures and large finite strains, which is predominantly frictional plastic. Copyright © 2001 John Wiley & Sons, Ltd.

KEY WORDS: finite element analysis; concrete; large deformation; plasticity; constitutive models; microplane model

1. INTRODUCTION

Under high hydrostatic pressures, concrete behaves as a plastic material capable of very large normal and shear strains, without a large volume change. Such strains are for instance observed in measurements and numerical simulations of impact of missiles into concrete walls, in explosive driving of anchors into concrete walls, in blast and ground shock effects on hardened protective structures, and in seismic response of highly confined concrete columns. Finite element modelling of such impact events requires knowledge of the stress–strain relations for concrete for finite strains at very large pressure.

There are numerous reports available in the literature about experimental works and studies conducted in order to investigate the mechanical response of concrete at high pressures.

*Correspondence to: Zdeněk P. Bažant, Northwestern University, Evanston, Illinois, 60208-3109, U.S.A.
†E-mail: z-bazant@northwestern.edu

Contract/grant sponsor: US Army Engineer WES; contract/grant number: DACA39-94-C-0025

Published online 11 September 2001

Received 17 December 1999
Revised 15 November 2000

Experiments by Woolson [1] at the beginning of the 20th century have shown that confinement in steel tubes causes concrete to exhibit plastic flow. Richart *et al.* [2] demonstrated the effect of confining pressure on the stress–strain curves. Later many other experiments have explored the ductile behaviour of concrete under high confining pressures and the effect of confinement by spiral rings, stirrups, glass or carbon fibres or polymer–fibre composites (e.g. References [3–16]).

However, the properties of concrete under very large deviatoric or shear strain have apparently not yet been experimentally determined. The triaxial tests and confined uniaxial tests considered so far can achieve very large hydrostatic pressures, but always with small strains and with shear angles not larger than 2–3°. In the computational practice, researchers usually simply extend, in one way or another, models calibrated for such small strains to the finite strain range, and then use them even when the computed shear angles attain 20–75°. Often they also arbitrarily introduce threshold values of stress and strain beyond which the material stiffness or strength are assumed to suddenly drop to zero.

Recently, Bažant *et al.* [17] presented the results of a new type of test of very large shear strains of concrete at very high pressures called the 'tube-squash' test. Owing to the confining pressure provided by a thick steel tube, a concrete specimen can achieve very large deviatoric strains without any visible fracturing or damage. The estimated shear angle at the centre of the specimen exceeds 70°. Such an experiment can be performed easily and offers a clear example of ductile behaviour of concrete at high pressures. It therefore appears to be an appealing source of information about the change of mechanical properties of concrete caused by high hydrostatic pressure.

Of course, in order for such an experiment to be meaningful, an efficient method of analysis of the test data must be available. Analysing the experimental results of the tube-squash test is not an easy task due to the strong geometric and material nonlinearities involved. Bažant *et al.* [17] proposed a simplified analysis based on the simultaneous solution of several non-linear equilibrium and compatibility equations.

A more accurate understanding of the phenomena occurring inside the concrete volume during the tube-squash test requires fitting the experimental data with a finite-strain finite element programme. To this end, an efficient and realistic constitutive model for concrete must be available. Its parameters may be adjusted, and thus their values leading to good representation of the tests may be identified.

This paper begins by a brief review of the tube-squash test (Section 1) and of the results of the simplified analysis originally proposed by Bažant *et al.* (Section 2). Sections 3–6 present a finite element analysis conducted employing microplane model constitutive relations for both materials involved in the tube-squash test, steel and concrete. The general concept of the microplane model formulation of constitutive laws is revisited in Section 4, where also a review of the models for steel and concrete is given. Section 5 discusses the generalization of the microplane model to finite strains, and finally Section 6 shows the results of the finite element analysis.

2. TUBE-SQUASH TEST FOR CONCRETE

The tube-squash test is a new type of test developed at Northwestern in 1997. The concrete specimen is cast inside a tube made of a highly ductile steel alloy, capable of large

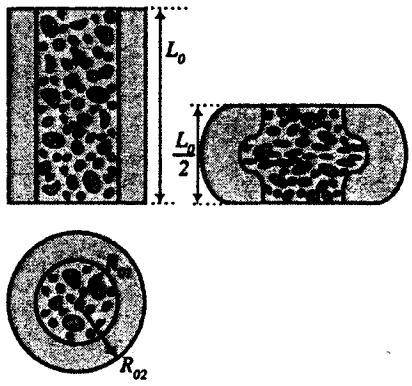

Figure 1. The specimen for the squash test. Steel tube filled with concrete.

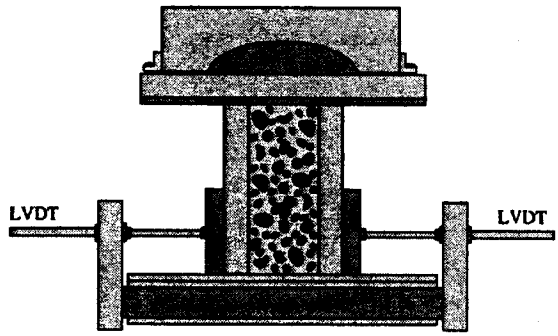

Figure 2. Experimental set-up for the squash test.

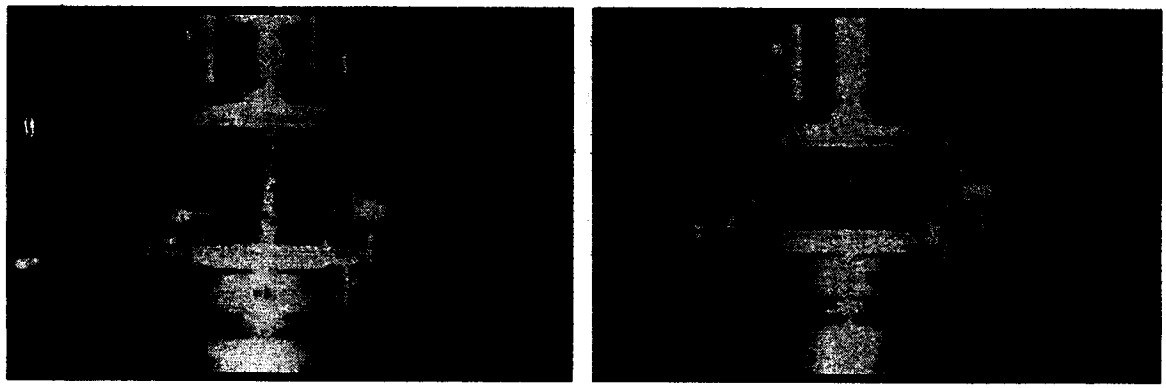

Figure 3. Pictures of the experimental set-up for the squash test.

deformation, up to 100 per cent, without cracking. After curing, the tube is then squashed up to one-half of its original length, causing the specimen to bulge.

Figure 1 shows cross-sections of one of the specimens used for the test, as it appears at the beginning and at the end of the test, after the loading process. Figures 2 and 3 show a schematic vertical cross-section and two pictures of the experimental set-up used for the test.

During the loading process, concrete inside the tube is subjected to extremely large strains while retaining its integrity (Figure 4). No visible cracks or voids can be observed on a cut through the specimens at the end of the test. Some damage, however, occurs in concrete at the microscopic level, as manifested by a reduction of Young's modulus, tensile strength and compressive strength after the test (all these quantities are reduced to approximately one-third of their original value).

The previous triaxial tests and confined uniaxial-strain compression tests achieve high pressures, but they cannot achieve large strains, neither shear nor normal. The tube-squash test can achieve very high normal strains and shear (or deviatoric) strains by allowing the specimen to deform highly nonuniformly. The penalty is a more complicated identification of the constitutive relation.

Figure 4. Saw-cut cross-sections of test specimens of a high-strength concrete filled tube and of an empty steel tube after the test.

Deformation and stresses inside the concrete volume would be hard to measure, and so they are not. To keep the test inexpensive and easy to perform, only a limited set of data are measured. The quantities measured during the test are the axial displacement under the load, the axial applied load and the lateral displacement of the tube at mid-height. Also the final shape of the specimen is recorded at the end of the test, after the specimen is cut longitudinally, in order to observe the inner profile assumed by the steel tube after deformation. Information about the stress and strain fields may be deduced from these data.

Two specimen sizes are tested: tubes of diameter of 76.2 mm (30 in) and 63.5 mm (2.5 in). The wall thickness is 14.22 mm (0.56 in) and 12.7 mm (0.5 in) respectively, the length of the tube is 88.9 mm (3.5 in) in both cases.

Tests have been conducted on tubes filled with normal strength and high strength concrete, hardened Portland cement paste and cement mortar, and on tubes with a snugly fitted limestone insert. All the specimens show remarkable plastic behaviour under extreme deformation. This study considers only high-strength concrete specimens, cast inside the smaller tubes (diameter 63.5 mm, thickness 12.7 mm).

As a companion test, also the empty steel tube is squashed in the same manner. The data obtained from such tests can be used to calibrate a material model for steel. This process is crucial, since a good accuracy is required in the analysis of the behaviour of steel during the squash test.

Figure 4 shows the photographs of cut cross-sections of a high strength concrete filled tube and of an empty steel tube specimen after 50 per cent axial shortening. Note how the inner profile of the deformed steel tube is affected by the presence of concrete. Also note how the aggregates have flattened during loading.

3. REVIEW OF SIMPLIFIED ANALYSIS AND ITS RESULTS

Bažant *et al.* [17] presented a relatively simple and fast method that can be used to deduce approximate stress–strain relations for concrete from the test data. Internal friction angles and the maximum shear angle achieved during the test can be estimated as well. Here only the

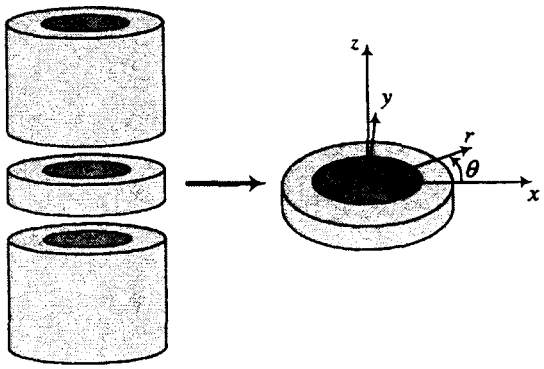

Figure 5. Co-ordinates definition for the analysis of a thin ring element at midlength of the tube.

basic concepts on which the method is based will be reviewed. For a detailed description of the theory and numerical implementation, see Reference [17].

The interesting feature of this simplified analysis is that no assumption has to be made on the constitutive law for concrete. The stresses inside the concrete volume can be estimated by means of equilibrium considerations.

The analysis is conducted by considering a thin circular element at midlength of the deformed tube as shown in Figure 5. Figure 5 also shows the co-ordinate system defined for the analysis. The steel is assumed to be governed by Hencky's total strain theory of plasticity, which is accurate enough in this case since the circular element considered in the analysis is assumed to deform symmetrically, with no rotation, and unloading is not expected to occur in this portion of the tube.

To take into account the effect of the bulging of the steel tube and of the non-uniform distribution of axial strain along the tube, some simplifying assumptions are made on the kinematics and on the distribution of stresses (σ_z, σ_θ are assumed to be uniformly distributed and σ_r is assumed to be varying linearly with r in steel and to be uniform in concrete).

By enforcing equilibrium conditions in the directions of r, θ and z, and by considering a number of compatibility conditions for the deformation of the tube, a system of 7 non-linear equations ($F_i = 0$, $i = 1, \ldots, 7$) can be obtained for the unknown stresses and strains in the circular element. This system is then solved by the Levenberg–Mardquardt iterative non-linear optimization algorithm, which minimizes the sum of squares $\sum_i F_i^2 = \text{Min}$. The whole loading process is analysed incrementally, by solving the system of equations at each step. This is done first for the test on the empty steel tube: in this case, the unknowns are not only the stresses and strains, but also the hardening function. Hencky's plasticity model for steel is thus calibrated. Then the test on the tube filled with concrete is analysed.

Some of the results obtained with this method are shown in Figure 6.

The algorithm just sketched is easy to implement and yields results in very short time. The drawback is that due to the simplified nature of this approach, the amount of information that can be obtained is limited. The average axial stress in concrete and the confining pressure at the contact point between steel and concrete can be estimated, but it is impossible to have a more accurate description of the stress field inside the concrete volume. A finite strain finite element analysis is desirable in order to get a more detailed description of the stress and strain

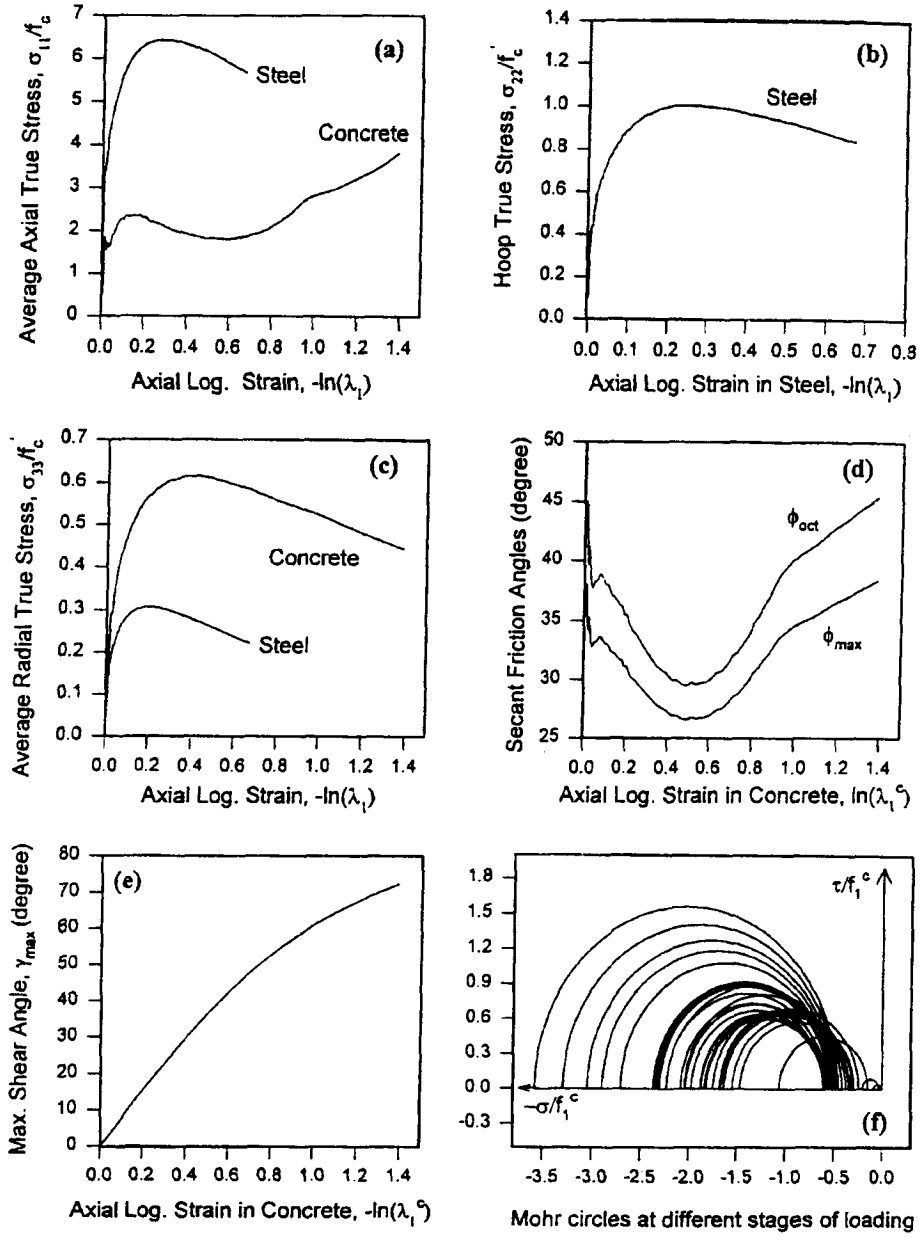

Figure 6. Results of simplified analysis.

fields. In addition to this, it must be emphasized that finite element analysis is necessary to get an idea of the error of the simplified analysis.

4. DESCRIPTION OF FINITE ELEMENT MODEL

As indicated in Reference [17], the aforementioned simplified approach could not capture the maximum pressure inside the concrete volume. The estimated confining pressure at the

contact point between concrete and steel is surprisingly low. This could be a manifestation of the fact that the stress distribution inside the concrete mass is highly non-homogeneous, and provides motivation for a more accurate analysis with FEM, which could offer a more complete description of the stress and strain fields. Such an analysis is also necessary in order to get an idea of the magnitude of the error of the simplified method.

Moreover, conducting a finite element analysis of the tube-squash test could provide a further validation of the microplane model for concrete and of its extension to the finite strain range.

The finite element analysis is performed in a standard way. The problem is two-dimensional, due to axial symmetry of the geometry. An explicit dynamic finite strain finite element programme has been developed, within an updated Lagrangian framework. The time integration is carried out using central differences and the quasi-static nature of the loading process is reproduced by employing dynamic relaxation. The novelty of this study is in the material models used for the computation, which are developed with the microplane approach, presented in the next section.

5. DESCRIPTION OF MATERIAL MODEL

For both concrete and steel, the material model is developed by using the microplane approach, which is proven to yield good results for concrete for both small and finite strain conditions. The microplane model is found to give a better performance also for steel, compared to classical tensor based plasticity models. About this aspect of the analysis see Reference [18] for further details.

5.1. History of microplane model

The background history of the microplane modelling approach can be traced back to a pioneering idea of Taylor [19], who proposed characterizing the constitutive behaviour of polycrystalline metals by relations between the stress and strain vectors acting on planes of all possible orientations within the material and determining the macroscopic strain and stress tensors as a summation of all these vectors under the assumption of a static or kinematic constraint. Batdorf and Budiansky [20] were the first to extend Taylor's idea and develop a realistic model for plasticity of polycrystalline metals, still considered among the best. Many other researchers subsequently refined or modified this approach to metals [21–26]. Extensions for the hardening inelastic response of soils and rocks were also made [27, 28].

All the aforementioned models used the so-called 'static constraint': the assumption that the stress vector acting on a given plane in the material, called the microplane, is the projection of the macroscopic stress tensor. Later Bažant [29], and Bažant and Oh [30] showed that, for stability reasons, a static constraint prevents the model from being generalized for post-peak behaviour or softening damage typical of quasi-brittle materials. The extension to softening damage requires replacing the static constraint by a kinematic constraint, in which the strain vector on any inclined plane in the material is the projection of the macroscopic strain tensor.

In all applications to metals, the formulations emanating from Batdorf and Budiansky's work were called the slip theory of plasticity. This form is however unsuitable for general material models, for example models of the cracking damage in quasibrittle materials, where

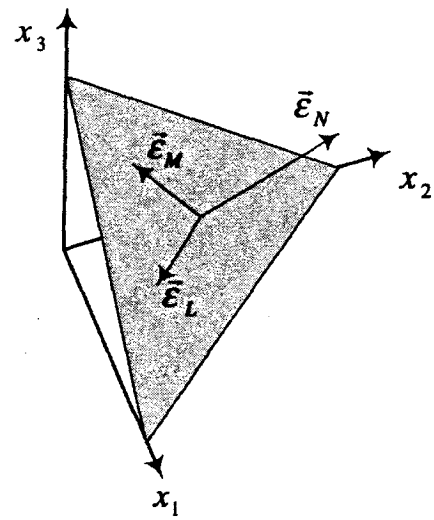

Figure 7. Strain components on a microplane.

the inelastic behaviour on the microscale does not physically represent plastic slip. For this reason the neutral term 'microplane model', applicable to any type of inelastic behaviour, was coined [29]. Microplane is the name given to a plane of any orientation in the material, used to characterize the microstructure of the material.

After generalizing the microplane model for both tensile and compressive damage [31, 32], the microplane model and the corresponding numerical algorithm reached its present, very effective formulation for concrete [33–35]. Microplane formulations have also been developed for anisotropic clays [36] and for soils [37–39]. A detailed review of the microplane model formulation with kinematic or static constraint can be found in Reference [40]. For both the formulations with kinematic and static constraints, the material properties are characterized by relations between the stress and strain components on the microplanes. The tensorial invariance restrictions need not be directly enforced in the constitutive relations, which is an advantageous feature of the microplane formulation. They are automatically satisfied by superimposing in a suitable manner the responses from the microplanes of all orientations. This is done by means of a variational principle (principle of virtual work) [29]. The fact that the constitutive law is described in terms of vectors rather than tensors endows the model with conceptual clarity and allows more realistic modelling of oriented phenomena such as friction or cracking. In the next sections we will present the basic formulation for the microplane model for the case of small strains. The generalization to the finite strain range will be discussed in Section 5.

5.2. Formulation with kinematic constraint

The orientation of a microplane is characterized by the unit normal $\mathbf{n}$ of components n_i (indices i and j refer to the components in Cartesian co-ordinates x_i). In the formulation with kinematic constraint, which makes it possible to describe softening in a stable manner, the strain vector $\vec{\varepsilon}_N$ on the microplane (Figure 7) is the projection of the macroscopic strain tensor ε_{ij}. So the components of this vector are $\varepsilon_{Ni} = \varepsilon_{ij} n_j$. The normal strain on the microplane is

$\varepsilon_N = n_i \varepsilon_{Ni}$, that is

$$\varepsilon_N = N_{ij}\varepsilon_{ij}, \quad N_{ij} = n_i n_j \tag{1}$$

where repeated indices imply summation over $i = 1,2,3$. The mean normal strain, called the volumetric strain ε_V, and the deviatoric strain ε_D on the microplane can also be introduced, defined as follows (for small strains):

$$\varepsilon_V = \varepsilon_{kk}, \quad \varepsilon_D = \varepsilon_N - \tfrac{1}{3}\varepsilon_V = \tfrac{2}{3}(\varepsilon_N - \varepsilon_S) \tag{2}$$

where ε_S = spreading strain = mean normal strain in microplane. ε_S characterizes the lateral confinement of the microplane and the creation of splitting cracks normal to the microplane. Considering ε_V and ε_D (or ε_S) is useful when dealing with the effect of lateral confinement on compression failure and when the volumetric–deviatoric interaction observed for a number of cohesive frictional materials, such as concrete, needs to be captured.

To characterize the shear strains on the microplane (Figure 7), one needs to define two co-ordinate directions M and L, given by two orthogonal unit co-ordinate vectors **m** and **l** of components m_i and l_i lying on the microplane. To minimize directional bias of **m** and **l** among microplanes, vectors **m** on different microplanes are chosen to be normal alternatively to axis x_1, x_2 or x_3.

The magnitudes of the shear strain components on the microplane in the directions of **m** and **l** are $\varepsilon_M = m_i(\varepsilon_{ij}n_i)$ and $\varepsilon_L = l_i(\varepsilon_{ij}n_i)$. Because of the symmetry of tensor ε_{ij}, the shear strain components may be written as follows [35, 41]:

$$\varepsilon_M = M_{ij}\varepsilon_{ij}, \quad \varepsilon_L = L_{ij}\varepsilon_{ij} \tag{3}$$

in which the following symmetric tensors are introduced:

$$M_{ij} = (m_i n_j + m_j n_i)/2, \quad L_{ij} = (l_i n_j + l_j n_i)/2 \tag{4}$$

Once the strain components on each microplane are obtained, the stress components are updated through microplane constitutive laws, which can be expressed in algebraic or differential form.

If the kinematic constraint is imposed, the stress components on the microplanes are equal to the projections of the macroscopic stress tensor σ_{ij} only in some particular cases, when the microplane constitutive laws are specifically prescribed so that this condition be satisfied. This happens for example in the case of elastic laws at the microplane level, defined with elastic constants chosen so that overall macroscopic behaviour is the usual elastic behaviour [40]. In general, the stress components determined independently on the various planes will not be related to one another in such a manner that they can be considered as projections of a macroscopic stress tensor. Thus static equivalence or equilibrium between the microlevel stress components and macrolevel stress tensor must be enforced by other means. This can be accomplished by application of the principle of virtual work, yielding

$$\sigma_{ij} = \frac{3}{2\pi}\int_\Omega \sigma_N n_i n_j \, d\Omega + \frac{3}{2\pi}\int_\Omega \frac{\sigma_{Tr}}{2}(n_i\delta_{rj} + n_j\delta_{ri})\, d\Omega \tag{5}$$

where Ω is the surface of a unit hemisphere. Equation (5) is based on the equality of the virtual work inside a unit sphere and on its surface, rigorously justified by Bažant *et al.* [41].

Table I. Weights and direction cosines for the 21-points integration formula.

α	n_1^α	n_2^α	n_2^α	w_α
1	0.18759474085	0	0.982246946377	0.019841269841
2	0.794654472292	−0.525731112119	0.303530999103	0.019841269841
3	0.794654472292	0.525731112119	0.303530999103	0.019841269841
4	0.187592474085	−0.850650808352	−0.491123473188	0.019841269841
5	0.794654472292	0	−0.607061998207	0.019841269841
6	0.187592474085	0.850650808352	−0.491123473188	0.019841269841
7	0.577350269190	−0.309016994375	0.755761314076	0.025396825396
8	0.577350269190	0.309016994375	0.755761314076	0.025396825396
9	0.934172358963	0	0.356822089773	0.025396825396
10	0.577350269190	−0.809016994375	−0.110264089708	0.025396825396
11	0.934172358963	−0.309016994375	−0.178411044887	0.025396825396
12	0.934172358963	0.309016994375	−0.110264089708	0.025396825396
13	0.577350269190	0.809016994375	−0.110264089708	0.025396825396
14	0.577350269190	−0.5	−0.645497224368	0.025396825396
15	0.577350269190	0.5	−0.645497224368	0.025396825396
16	0.356822089773	−0.809016994375	0.467086179481	0.025396825396
17	0.356822089773	0	−0.934172358963	0.025396825396
18	0.356822089773	−0.809016994375	0.467086179481	0.025396825396
19	0	−0.5	0.866925403784	0.025396825396
20	0	−0.5	−0.866925403784	0.025396825396
21	0	1	0	0.025396825396

The integration in Equation (5), is performed numerically by an optimal Gaussian integration formula for spherical surface using a finite number of integration points on the surface of the hemisphere, which may be expressed in the form

$$\int_\Omega f(\mathbf{x})\,\mathrm{d}\Omega = \sum_{\alpha=1}^{N} w_\alpha f(\mathbf{x}_\alpha) \tag{6}$$

in which w_α are weights and N is the number of numerical integration points. Such an integration technique corresponds to considering a finite number of microplanes, one for each integration point. A optimal Gaussian integration formula consisting of 28 integration points is given by Stroud [42]. Bažant and Oh [43] developed a more efficient and about equally accurate optimal Gaussian formula with 21 integration points, and studied the accuracy of various formulas in different situations encountered in material modelling. The values for the weights and the direction cosines of the unit normal vectors $\mathbf{n}^\alpha$ for the 21 point formula are given in Table I.

5.3. Formulation with static constraint

A formulation with static constraint equates the stress components on each microplane to the projections of the macroscopic stress tensor σ_{ij}. Once the strain components on each microplane are updated by the use of the microplane constitutive laws, the macroscopic strain tensor is obtained again by applying the principle of virtual work.

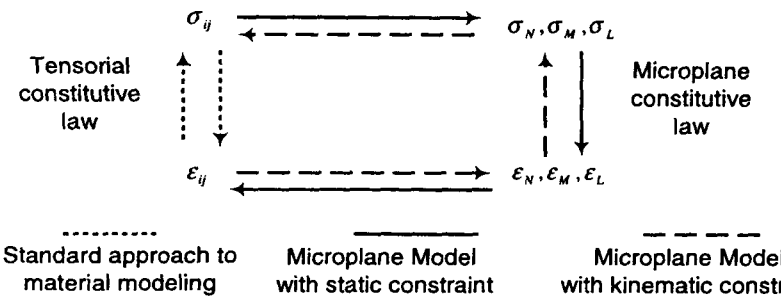

Figure 8. Patterns for stress or strain update in the microplane model with static or kinematic constraint.

The microplane components of stress are defined as follows:

$$\sigma_N = N_{ij}\sigma_{ij}, \quad N_{ij} = n_i n_j \tag{7}$$

$$\sigma_M = M_{ij}\sigma_{ij}, \quad \sigma_L = L_{ij}\sigma_{ij} \tag{8}$$

where

$$M_{ij} = (m_i n_j + m_j n_i)/2, \quad L_{ij} = (l_i n_j + l_j n_i)/2 \tag{9}$$

The complementary virtual work equation provides, in analogy to Equation (5),

$$\varepsilon_{ij} = \frac{3}{2\pi}\int_\Omega \varepsilon_N n_i n_j \, d\Omega + \frac{3}{2\pi}\int_\Omega \frac{\varepsilon_{Tr}}{2}(n_i\delta_{rj} + n_j\delta_{ri})\, d\Omega \tag{10}$$

Again, volumetric and deviatoric quantities can be introduced:

$$\sigma_V = \sigma_{kk}/3, \quad \sigma_D = \sigma_N - \sigma_V \tag{11}$$

σ_V and σ_D are used when the effect of hydrostatic pressure and spreading stress or confining stress need to be accounted for explicitly.

5.4. Formulation with double constraint

It is possible and advantageous to formulate the microplane model with particular material laws such that a kinematic constraint for the strains coexists with a static constraint for the true stresses in the sense of damage mechanics (but of course not with the actual stresses). When this happens the model is said to have a *double constraint* since it satisfies simultaneously the integral equations (5) for true stresses and (10) for strains. Such a double constraint is useful in microplane damage formulations [35, 40, 41]. If damage variables are introduced on the microplanes [31], then such a constraint allows formulating an uncoupled fourth-order damage tensor that involves no other constitutive variables than the damage.

Figure 8 shows schematically the pattern followed in order to update the stress or strain in the microplane model approach. As shown, the microplane model takes simple constitutive laws on each microplane and transforms them into a consistent three-dimensional model. In this work, the kinematic constraint is used. The numerical procedure is incremental and small increments in stress are taken at each step. At each step, the procedure to update the stress tensor is the following:

1. The macroscale strain tensor is projected onto the 21 microplanes using Equations (1)–(4).
2. Constitutive laws are applied on each microplane producing the stresses on each of the 21 microplanes. Such constitutive laws are in the form

$$\sigma_l = F_i(\varepsilon_D, \varepsilon_L, \varepsilon_M, \Delta\varepsilon_D, \Delta\varepsilon_L, \Delta\varepsilon_M, \varepsilon_V, \Delta\varepsilon_V, \ldots), \quad i = D, L, M, V \tag{12}$$

3. The macroscopic stress is then determined numerically via integration of Equation (5).

5.5. *Advantages of microplane model*

Developing a constitutive model with the microplane approach offers several advantages with respect to the standard approach in which the constitutive law is expressed in terms of stress and strain tensors and their invariants. We briefly list here some of these advantages (a more accurate discussion on this aspect can be found, e.g. in References [35] and [35a]):

- The constitutive law is written in terms of vectors rather than tensors.
- Tensorial invariance in the constitutive law is automatically satisfied.
- It is possible to describe directional strain localization.
- Phenomena such as slip, friction, crack opening, can be directly characterized on the surface where they take place.
- It is possible to naturally reproduce vertex effect and deviation from normality, because prescribing constitutive laws independently on many planes of different orientations corresponds to a multisurface plasticity formulation.
- The kinematic constraint automatically provides all the major cross-effects (e.g. dilatancy, pressure sensitivity) as a result of the interaction among planes.
- Combination of loading and unloading on different microplanes allows reproducing phenomena such as hysteresis under cyclic loading and Bauschinger effect.
- The model is distinguished by conceptual simplicity. All the quantities involved in the formulation have a precise physical meaning (such as friction, slip, cracking or splitting in a certain direction, confinement, pore collapse, etc.). Complicated three-dimensional constitutive behaviour can be effectively modelled in terms of vectors rather than tensors by focusing on simple relations between stress and strain components on a plane. Having to deal with the relationship between the microplane components and the macrolevel tensors of course involves more computational work than just dealing with tensorial quantities, but this aspect has to be taken care of only once for all the models. Once the algorithm for the numerical integration of Equations (5) or (9) is established, the microplane model provides a very efficient theoretical and numerical framework that can be used for developing any kind of material model.

The disadvantage of this approach is a larger amount computations. The number of variables to be stored at each integration point is higher than that required when using tensorial constitutive laws. However, the increase in computational burden due to the material subroutine has been made much less significant by the increases in computational power, and has little importance in the case of large-scale computations, for which the most of the computational cost arises from the solution of the system.

5.6. *Concrete*

The microplane model for concrete is the result of almost two decades of studies by Bažant and coworkers. The version adopted for the analysis presented in this paper is referred to as M4 and a complete description of it can be found in References [35] and [35a].

The model is formulated by use of simple one-to-one relations between one stress component and the associated strain component. Except for a frictional yield surface, cross dependencies are not accounted for explicitly, but appear in the model as result of the interaction among planes.

The model parameters are divided into a few adjustable ones (only four are needed) and many non-adjustable ones (of which twenty are used), common to all concretes. Bažant *et al.* [35] provide an efficient procedure to identify the model parameters in a systematic way from test data. Creep and rate-effect have also been introduced in M4, but are neglected in this study.

Each constitutive relationship at the microplane level is expressed by introducing stress–strain boundaries (strain-independent yield limits): at every step of the incremental computation a trial elastic value is computed for each component of stress. If such trial value exceeds the boundary for that component, the correct stress is obtained by dropping the trial stress at constant strain to the surface of the boundary. Despite the abrupt change of slope when the stress reaches the boundary, the macroscopic response is quite smooth, because different microplanes enter the loading or unloading regime at different times.

A thorough discussion of the stress–strain boundaries for M4 is given in Reference [35]. The boundaries for each microplane stress component are given as functions of the corresponding microplane strain component. A list of the boundaries is given in the following.

The strain softening tensile normal boundary is given as

$$\sigma_N^b = F_N(\varepsilon_N) = Ek_1c_1 \exp\left(-\frac{\langle \varepsilon_N - c_1c_2k_1 \rangle}{k_1c_3 + \langle -c_4(\sigma_V/E_V) \rangle}\right) \tag{13}$$

where the superscript b refers to the stress on the boundary, and the Macauley brackets are defined as $\langle x \rangle = \mathrm{Max}(x, 0)$.

The compressive deviatoric boundary controls the axial crushing strain of concrete in compression when the lateral confinement is too weak to prevent crushing. The tensile deviatoric boundary simulates the transverse crack opening of axial distributed cracks in compression and controls the volumetric expansion and lateral strains in unconfined compression tests. These two boundaries are, respectively, given as

$$\text{for } \sigma_D > 0: \quad \sigma_D^b = F_D(\varepsilon_D) = \frac{Ek_1c_5}{1 + (\langle \varepsilon_D - c_5c_6k_1 \rangle / k_1c_{20}c_7)^2} \tag{14}$$

$$\text{for } \sigma_D < 0: \quad \sigma_D^b = F_D(-\varepsilon_D) = -\frac{Ek_1c_8}{1 + (\langle -\varepsilon_D - c_8c_9k_1 \rangle / k_1c_7)^2} \tag{15}$$

Experimental data for unconfined tension and compression display smooth rounded peaks, which suggests the existence of a limited capacity for yield. To capture this phenomenon, additional horizontal boundaries (i.e. strain-independent boundaries) are included for the tensile normal stress and the tensile and compressive deviatoric stresses on the microplanes.

These horizontal boundaries also allow an accurate description of hysteretic loops under cyclic loading.

The shear boundary represents a non-linear frictional yield condition, giving the dependence of the shear yield stress on the normal stress σ_N. For simplicity, the frictional boundary is applied not to the resultant shear stress on each microplane, but to the components σ_L and σ_M separately. It is seen that the random distribution of directions M and L on the various microplane, compensates for the directional bias that might be introduced by this simplification. The shear boundary depends also on the volumetric strain ε_V. When the volumetric strain is small the boundary provides a finite cohesive stress, which decreases to zero with increasing volumetric strain. The friction boundary is expressed as

$$\sigma_V^b = F_T(-\sigma_N) = \frac{E_V k_1 k_2 c_{10} \langle -\sigma_N + \sigma_N^0 \rangle}{E_V k_1 k_2 + c_{10} \langle -\sigma_N + \sigma_N^0 \rangle} \tag{16}$$

where

$$\sigma_N^0 = \frac{E_V k_1 c_1}{1 + c_{12} \langle \varepsilon_V \rangle} \tag{17}$$

Note that $\lim_{\sigma_N \to \infty} \sigma_V^b = E_V k_1 k_2$ which represents a horizontal asymptote. This means that, at very high confining pressures, concrete becomes a frictionless plastic material.

Finally, volumetric boundaries, tensile and compressive, are used, in the form

$$\text{for } \sigma_V > 0: \quad \sigma_V^b = F_V^+(\varepsilon_V) = \frac{E_V k_1 c_{13}}{1 + (c_{14}/k_1)\langle \varepsilon_V - c_{13} c_{15} k_1 \rangle} \tag{18}$$

$$\text{for } \sigma_V < 0: \quad \sigma_V^b = F_V^-(\varepsilon_V) = -E k_1 k_3 \exp\left(-\frac{\varepsilon_V}{k_1 k_4}\right) \tag{19}$$

The effect of material damage on the incremental elastic stiffness is taken into account by introducing empirical rules for the incremental unloading moduli on the microplanes. Unloading is assumed to occur when the work rate $\sigma \dot{\varepsilon}$ becomes negative, and this unloading criterion is considered separately for each microplane component. The following rules are used:

$$\text{for } \varepsilon_V \leqslant 0 \quad \text{and} \quad \sigma_V \leqslant 0: \quad E_V^U(-\varepsilon_V, -\sigma_V) = E_V \left(\frac{c_{16}}{c_{16} - \varepsilon_V} + \frac{\sigma_V}{c_{16} c_{17} E_V} \varepsilon_V \right) \tag{20}$$

$$\text{for } \varepsilon_V > 0 \quad \text{and} \quad \sigma_V > 0: \quad E_V^U(\varepsilon_V, \sigma_V) = E_V \left(1 + c_{18} \frac{\sigma_V}{E_V} \varepsilon_V \right) \tag{21}$$

$$E_D^U = (1 - c_{19}) E_D + c_{19} E_D^S \tag{22}$$

$$\text{where if } \sigma_D \varepsilon_D \leqslant 0: \quad E_D^S = E_D \quad \text{else } E_D^S = \text{Min}(\sigma_D/\varepsilon_D, E_D) \tag{23}$$

$$E_T^U = (1 - c_{19})E_V + c_{19}E_V^S \tag{24}$$

$$\text{where if } \sigma_V \varepsilon_V \leqslant 0: \quad E_T^S = E_T \quad \text{else } E_T^S = \text{Min}(\sigma_T/\varepsilon_T, E_T) \tag{25}$$

5.7. *Steel*

Several possible plasticity models can be easily implemented with the microplane approach. Carol and Bažant [40] and Brocca and Bažant [18] have shown that by choosing appropriate constitutive laws at the microplane level it is possible to develop a microplane model version of J_2 incremental plasticity with a kinematic constraint. Using a static constraint it is possible to implement a version of the microplane model analogous to the slip theory of plasticity of Batdorf and Budiansky [20]. The difference from the slip theory of plasticity is given by how the micro–macro constraints are dealt with [18].

Since steel does not exhibit strain softening, the kinematic constraint is not necessary. But for analysing the squash test it is desirable to have a constitutive model for steel with the kinematic constraint, which can be more efficiently implemented in an explicit finite element code. J_2 incremental plasticity models cannot reproduce the vertex effect (deviation from normality) for non-proportional loading paths. Therefore, a kinematically constrained microplane model is developed, in order to reproduce the vertex effect. This is achieved by prescribing independent yield conditions for the shear quantities and the deviatoric parts of the normal quantities at the microplane level (see Reference [18] for details). Yielding is assumed to occur when either one of the following conditions is met:

$$\begin{aligned} f_a &= \sigma_V^2 + \sigma_M^2 - k_a^2 = 0 \\ f_b &= \sigma_D^2 - k_b^2 = 0 \end{aligned} \tag{26}$$

where

$$\sigma_D = \sigma_N - \sigma_V, \quad \sigma_V = \sigma_{kk}/3 \tag{27}$$

k_a, k_b are two hardening parameters, functions of the plastic strains, specified independently and calibrated using the results of the test on the empty steel tube.

The capability to capture the vertex effect is crucial in stability problems where the non-proportionality in the loading path is sudden and sharp. However, even in the case of the tube-squash test, due to material rotation in the shear bands of the deformed tube, the local stresses in a material element increase non-proportionally and the microplane model with the two yield conditions (26) yields a more accurate result than the standard J_2 incremental plasticity [18].

6. GENERALIZATION TO LARGE FINITE-STRAINS AND DEFINITIONS OF STRESS AND STRAIN

A systematic and detailed discussion about how to extend the microplane model to very large strains (of the order of 100 per cent) is given by Bažant *et al.* [33]. Only a brief review of the main concepts on which such an extension in based is given here.

The choice of strain measure needs to be discussed. One may consider a broad class of tensors called the Doyle–Ericksen tensors [44–46]:

$$\text{for } m \neq 0\text{: } \varepsilon^{(m)} = \frac{1}{m}(\boldsymbol{U}^m - \boldsymbol{I}) \quad \text{for } m = 0\text{: } \varepsilon^{(m)} = \ln \boldsymbol{U} \tag{28}$$

where $\boldsymbol{U} = \sqrt{\boldsymbol{C}}, \boldsymbol{C} = \boldsymbol{F}^{\mathrm{T}}\boldsymbol{F}$, and parameter m could be any real number. $\boldsymbol{C}$ is the Cauchy–Green deformation tensor: $\boldsymbol{U}$ is the right-stretch tensor, defined by the polar decomposition $\boldsymbol{F} = \boldsymbol{R}\boldsymbol{U}$ of the deformation gradient $\boldsymbol{F} = \partial \boldsymbol{x}/\partial \boldsymbol{X}$, where $\boldsymbol{x}$ and $\boldsymbol{X}$ are as usual the final and initial Cartesian co-ordinates of the material point [45–47]. (The tensor products such as $\boldsymbol{RU}$ are singly contracted products, i.e. the dot symbol for product is omitted.)

For $m = 2$, Equation (28) gives the Green's Lagrangian strain tensor [47]:

$$\varepsilon = \tfrac{1}{2}(\boldsymbol{F}^{\mathrm{T}}\boldsymbol{F} - \boldsymbol{I}) \tag{29}$$

For $m = 1$, Equation (28) yields the Biot strain tensor, and for $m \to 0$ the Hencky (logarithmic) strain tensor [45, 46, 48]. The stress tensor $\boldsymbol{S}$ for which $\boldsymbol{S} : \mathrm{d}\varepsilon$ according to (29) is the correct work expression (called the conjugated stress tensor) is the second Piola–Kirchhoff stress tensor, which is related to the Cauchy (true) stress tensor σ by the following relations:

$$\boldsymbol{S} = \boldsymbol{F}^{-1}J\sigma\boldsymbol{F}^{-1} \quad \text{or} \quad \sigma = J^{-1}\boldsymbol{F}\boldsymbol{S}\boldsymbol{F}^{\mathrm{T}} \tag{30}$$

where $\boldsymbol{F}^{-\mathrm{T}} = (\boldsymbol{F}^{-1})^{\mathrm{T}} = (\boldsymbol{F}^{\mathrm{T}})^{-1}$ [45–47].

The decomposition of large deformations into their volumetric and deviatoric parts is, in general, multiplicative. It has the form $\boldsymbol{U} = \boldsymbol{F}_D\boldsymbol{U}_V$ [49–54] where $\boldsymbol{U}$ = right stretch tensor, $\boldsymbol{U}_V$ = volumetric right stretch tensor, and $\boldsymbol{F}_D$ = deviatoric transformation tensor. For concrete and many other materials, the volumetric–deviatoric decomposition is simplified by the fact that the volume changes are always small. In that case the decomposition can approximately be written as additive [55]. In component form it reads $\varepsilon_{ij} = \varepsilon_{Dij} + \varepsilon_V\delta_{ij}$, where ε_V is the exact expression for the volumetric strain for a given strain measure. For Green's Lagrangian strain measure, $\varepsilon_V = \varepsilon_0 + \frac{1}{2}\varepsilon_0^2$, with $\varepsilon_0 = (J-1)/3$ ($J = \det \boldsymbol{F}$ = Jacobian of the transformation) and the additive approximation is acceptable up to a volume change of 3 per cent. For Biot strain measure $\varepsilon_V = J^{1/3} - 1$, and the approximation is acceptable up to a volume change of 8 per cent. The additive decomposition is exact if and only if the strain measure is the Hencky (logarithmic) strain tensor $\boldsymbol{H}$, in which case $\varepsilon_V = (\ln J)/3$. For concrete, the volume change is -3 per cent at the highest pressures tested so far (300 000 psi, or 2069 MPa: [16]). Thus the classical multiplicative decomposition, which is less practical for calculation than the additive decomposition, seems to be inevitable only for materials exhibiting very large volume changes, such as stiff foams.

Bažant and coauthors [33] show that for an efficient and appropriate formulation of a microplane constitutive model, the best choice of strain tensor is the Green's Lagrangian strain tensor, while the appropriate stress tensor is the back-rotated Cauchy (true) tensor. Although these strain and stress tensors are non-conjugate, they can still be admissible because the following four conditions are satisfied: (1) there is a unique correspondence between the non-conjugate constitutive law and the conjugate constitutive law in terms of Green's Lagrangian strain tensor; (2) if a micro–macro kinematic constraint of microplane model is imposed in terms of one type of strain tensor, a kinematic constraint is satisfied for any other finite strain tensor; (3) the elastic parts of strains are always small, which ensures the energy dissipation

caused by elastic deformation formulated in terms of nonconjugate stress and strain tensors to be always negligible and (4) the inelastic stress drops to the yield or boundary surface, used in the time step numerical solution, occur at constant strain and always dissipate energy. For a detailed discussion on these four conditions see Reference [33]. The motivations of the choice of the back-rotated Cauchy stress and the Green's Lagrangian strain tensor will now be discussed.

6.1. Choice of the stress tensor for the microplane model

To fully exploit the advantage of formulating a material constitutive model terms of vectors rather than tensors, it is necessary that the stress components on the microplane alone suffice to characterize the *true* stress on each microplane. Only if this condition is satisfied it is possible to use directly the normal and shear components on the microplanes to express inelastic phenomena such as friction, slip, cracking stress, confinement, axial splitting and yield limit.

It can be shown that for large stretches such as 2 or $\frac{1}{2}$, the components of the second Piola–Kirchhoff stress tensor can enormously differ from the corresponding components of the Cauchy stress tensor, easily by a factor of 2 or even in the sign. Consequently, the limit condition of frictional slip on a certain plane cannot be formulated in terms of the components of $\boldsymbol{S}$ on one microplane, and neither can the limit conditions of yield or strength limit, or the law of strain hardening on that plane. Frictional slip on a certain plane, for example, depends on the true normal and shear stresses on a section by that plane through the deformed material, and not directly on the stresses transformed to this section of the material in its virgin initial state. Similar conclusions can be reached for other easily calculated stress tensors conjugated to other finite strain tensors, such as Biot's tress tensor. Another relevant observation to be made is that a constitutive law in terms of the second Piola–Kirchhoff stress does not allow simple control of hydrostatic pressure and spreading stress, and thus also of pressure sensitivity, confinement, internal friction and dilatancy of material. Further examples of difficulties with the use of $\boldsymbol{S}$ to express the yield limit in shear and the internal friction angle have been given by Bažant [56]. Again, similar difficulties can be demonstrated for stresses conjugate to other finite strain tensors, e.g. Biot's.

The Cauchy stress tensor would give a clear physical meaning for the microplane stress components, but it cannot be used in a constitutive equation for a solid with memory of the initial state because it is not referred to the initial configuration and is not associated by work to any Lagrangian finite strain tensor. It is conjugate to the deformation rate (or velocity strain) and could be applied only in Eulerian or updated Lagrangian approaches, which do not keep track of the initial state as the strain measure is path-dependent.

The proper stress tensor to use is the Cauchy stress tensor rotated back to the initial co-ordinates $\boldsymbol{X}$ attached to the material, called the back-rotated Cauchy stress tensor and expressed as

$$\boldsymbol{s} = \boldsymbol{R}^{\mathrm{T}} \sigma \boldsymbol{R} \tag{31}$$

where σ is the Cauchy stress tensor, and $\boldsymbol{R}$ is the material rotation tensor. In the case of no rotation, $\boldsymbol{s}$ coincides with the Cauchy stress tensor. If there is rotation $\boldsymbol{R}$, the physical meaning of stresses does not get changed by it, only the component values get transformed. The hydrostatic pressure, which is important for pressure sensitive materials such as concrete,

is given by $\mathrm{tr}(\boldsymbol{s})$. Only for the Cauchy stress tensor, the actual stresses acting on a microplane can be expressed solely from the stress tensor projection on that plane.

Another attractive choice may seem to be the back-rotated Kirchhoff stress tensor (not considered here), used by Hoger [57], Eterovic and Bathe [58] and Gabriel and Bathe [59]. It is also used in ABAQUS [60]. But for these and other stress definitions, the tensor projections on the microplane do not represent the actual stresses acting on the microplane. Their calculation requires the use of the entire stress tensor.

A constitutive relation written in terms of the back-rotated Cauchy stress or back-rotated Kirchhoff stress can, of course, be always transformed to a constitutive relation in terms of the second Piola–Kirchhoff stress. But after this transformation, the constitutive law can no longer be expressed separately in terms of stress and strain vectors on one microplane. It is much more complicated and hard to use in data fitting.

6.2. Choice of strain tensor for microplane model

The first natural choice for the strain measure would be the strain tensor that is work conjugate to the chosen stress tensor. In the case of the microplane model this is not possible for two reasons [33].

The first reason is that the strain tensors conjugate to the back-rotated Cauchy stress and back-rotated Kirchhoff stress are both nonholonomic. In other words, they depend not only on the current deformation gradient, but also on the deformation path in which the current state has been reached. A path-dependent strain tensor, although widely used in updated Lagrangian formulations for finite strain plasticity of metals, appears questionable for materials for which the initial virgin state is an important reference for defining the constitutive behaviour, such as fracturing and damage in concrete.

The second reason is that, in a finite strain generalization of the microplane model, a definite physical meaning needs to be attached to the normal and shear strain components on the microplanes. The following two conditions must be met:

Condition I. The normal strain component e_N on a microplane should uniquely characterize the stretch λ_N of a material line segment whose direction $\boldsymbol{n}$ is initially normal to the microplane. It should be independent of the stretches of material line segments in other initial directions.

Condition II. The shear strain component θ_{NM} (or θ_{NL}) should uniquely characterize the change of angle θ_{NM} or θ_{NL} between two initially orthogonal material line segments with initial unit vectors $\boldsymbol{n}$ and $\boldsymbol{m}$. It should be independent of the stretch in any direction and of the angle change in planes other than $(\boldsymbol{n},\boldsymbol{m})$ or $(\boldsymbol{n},\boldsymbol{l})$.

Only the Green's Lagrangian strain meets these two conditions [33]. For any other strain measure, the shear angle and the normal stretch cannot be calculated solely from the components of the strain tensor on the same microplane. Rather, the entire strain tensor needs to be used for that purpose.

7. RESULTS

The hardening parameters k_a, k_b employed in the model for steel are tuned using the results of the companion test on the empty steel tube. Figure 9 shows a three-dimensional visualization

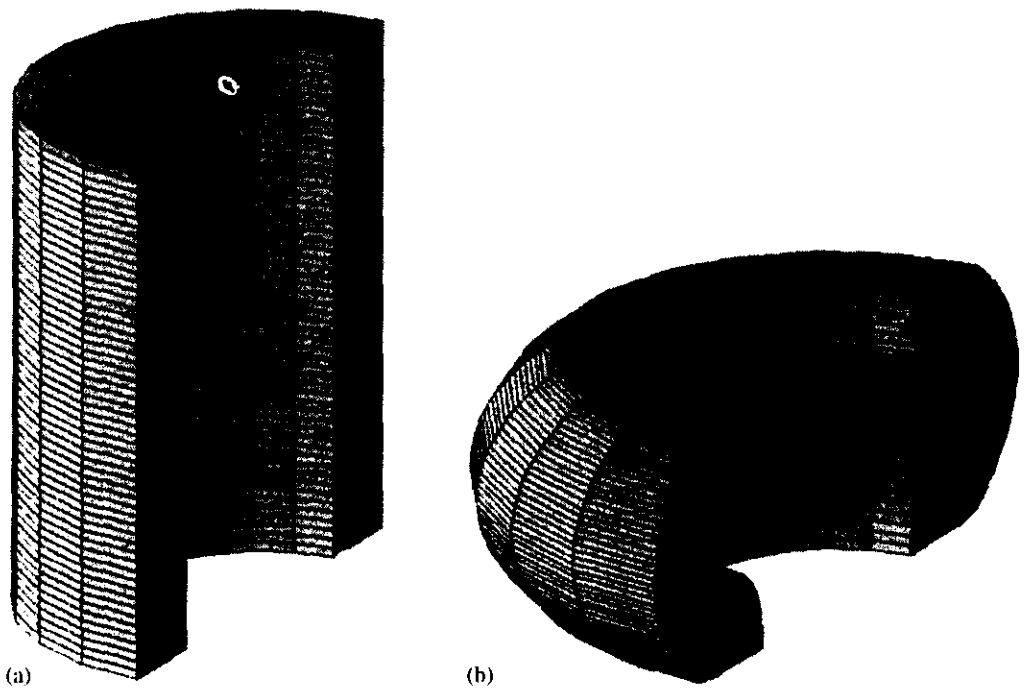

Figure 9. Three-dimensional visualization of the mesh used for the analysis on the empty tube: (a) undeformed; and (b) at the end of the loading process.

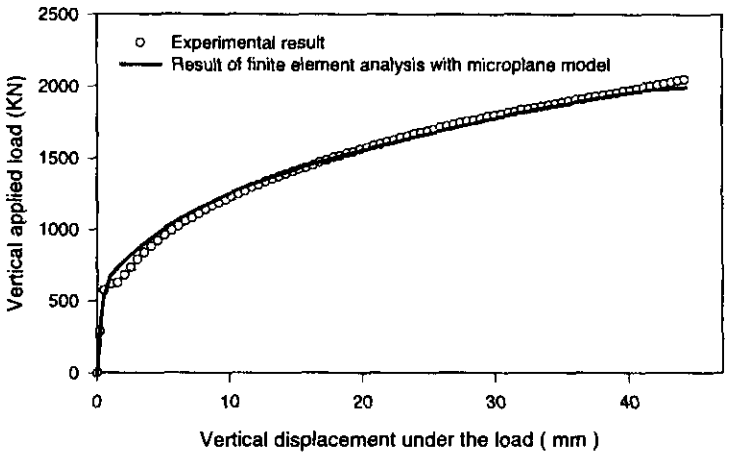

Figure 10. Experimental and computed load–displacements diagram for the empty tube.

of the mesh used for the analysis of the steel tube and the deformed mesh at the end of the process. Figure 10 shows a comparison of the experimental load–displacement diagram with the one obtained by finite element analysis. Clearly, the material parameters can be adjusted so that the experimental curve be fitted very accurately.

The results of the analysis of the concrete filled tube are shown in the following figures. Figure 11 shows the initial and deformed mesh and Figure 12 gives the load–displacement

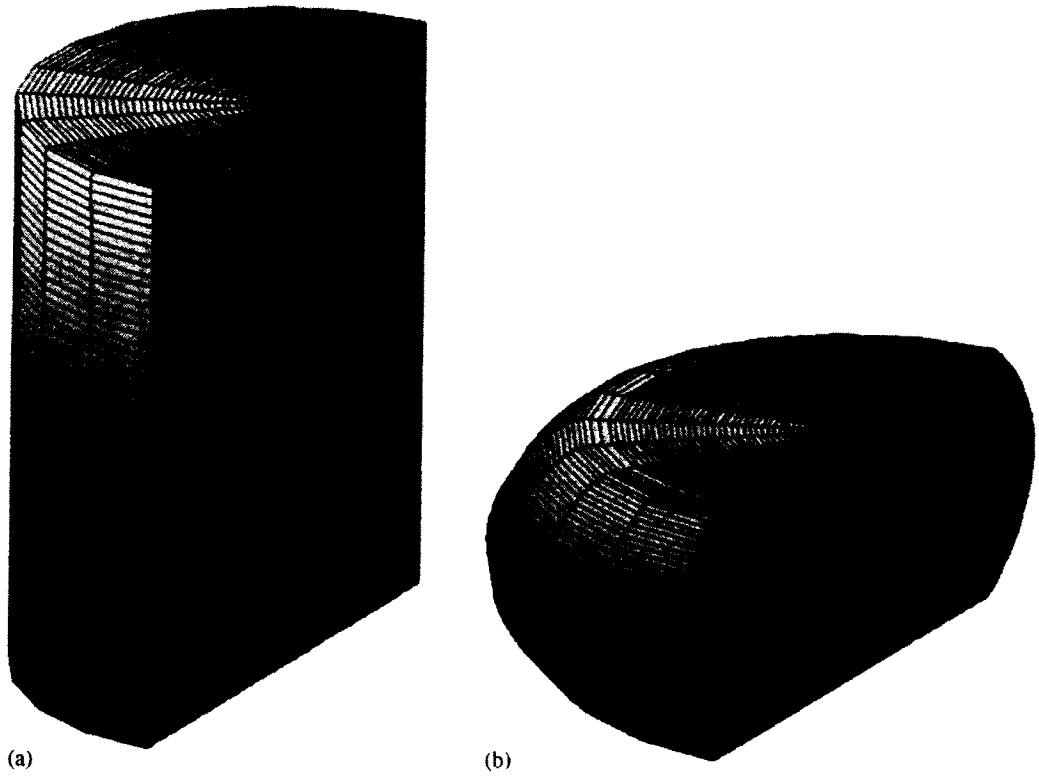

Figure 11. Three-dimensional visualization of the mesh used for the analysis on the tube filled with concrete: (a) undeformed; and (b) at the end of the loading process.

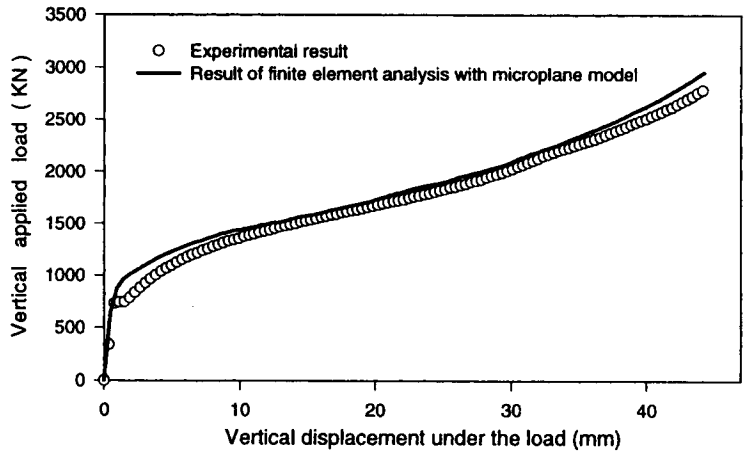

Figure 12. Experimental and computed load–displacements diagram for the tube filled with concrete.

curve. In this case it was sufficient to adjust merely the parameter for compressive strength in the microplane model for concrete in order to reproduce very closely the mechanical behaviour of the specimen observed experimentally. That no other adjustments were needed is remarkable.

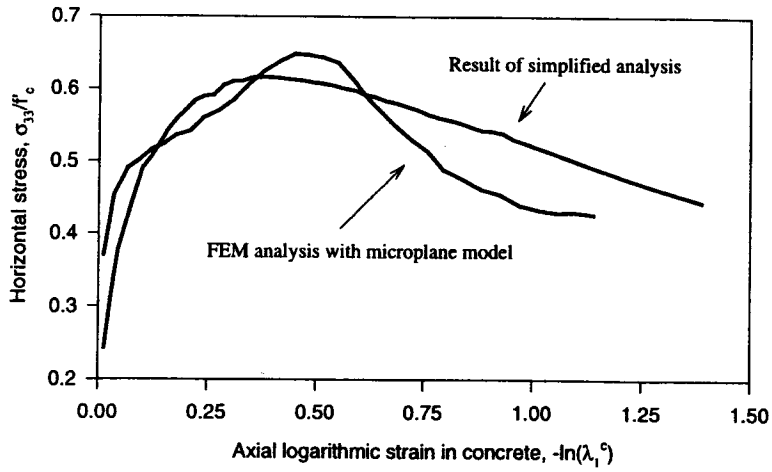

Figure 13. Confining pressure at the contact point between steel and concrete.

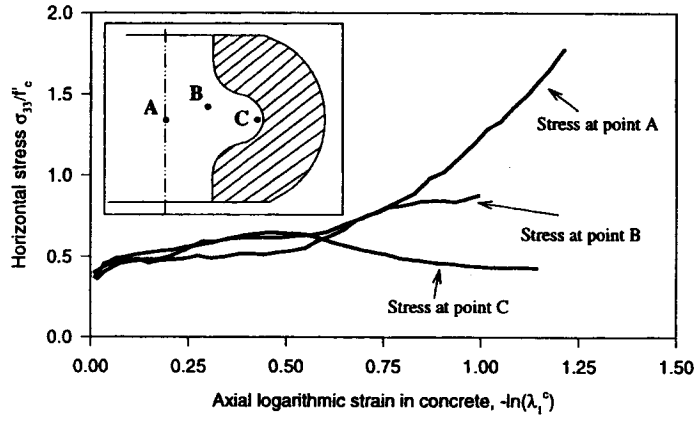

Figure 14. Computed radial compressive stress in concrete at three different points.

Figure 13 shows a comparison of the confining pressure at the contact point between concrete and steel at midlength of the specimen, as evaluated by the simplified analysis reviewed in Section 2.

The two curves exhibit an excellent agreement and both give a rather low value of maximum confining pressure at that point (about $0.6 \times$ compressive strength of concrete). As expected this is not the highest confining pressure experienced by concrete. Figure 14 shows the radial stress in concrete calculated at three different distances from the axis of the specimen.

At the axis, the radial stress reaches about $1.8f_c$, while the axial stress is about $8f_c$, and the volumetric (hydrostatic) stress component is about $3.9f_c$.

The maximum shear angle, which occurs at point A, is obtained for the end of the test as 71.5°. The simplified analysis in Reference [17] led to the estimate of 70°, which is very close.

8. CONCLUSIONS

1. The experimental data can be fitted quite closely by the finite element computational model. Both the load–displacement curves and the final deformed shapes of the specimens are satisfactorily reproduced.
2. This result provides a validation of the microplane model. Especially, the model is proven capable of reproducing the response of concrete even at very high pressures and very large shear angles (up to 70°).
3. Owing to the availability of numerical simulation of the tube squash test with a realistic material model such as the microplane model, finite element analysis makes if possible to assess the effectiveness of the previously proposed simplified method for evaluating the results of the tube-squash test. It is shown that this simplified method yields results in reasonable agreement with the present finite element analysis, especially in terms of the confining pressure and the shear angle. It can therefore be considered as a viable simplified method for extracting information from the tube-squash test about the mechanical behaviour of concrete at extreme pressures and very large shear strains.
4. It should be noted that incorporation of the rate effect would be needed in order to simulate with the same model both the tube-squash test and impact on concrete walls.

ACKNOWLEDGEMENTS

Support of the background research of the microplane model by the U.S. Army Engineer Waterways Experiment Station (WES), Vicksburg, Mississippi, under contract DACA39-94-C-0025 with Northwestern University is gratefully acknowledged.

REFERENCES

1. Woolson IH. Some remarkable tests indicating flow in concrete under pressure. *Engineering News* 1905; **54**(18):459–460.
2. Richart FE, Branzaeg A, Brown RL. Failure of plain and spirally reinforced concrete in compression. *Engineering Experiment Station Bulletin, University of Illinois, Urbana* 1929; **190**:79.
3. Balmer GG. Shearing strength of concrete under high triaxial stress—computation of Mohr envelope as a curve. *Report SP*-23, Structural Research Laboratory, Bureau of Reclamation. U.S. Department of the Interior. Denver, Co, 1949.
4. Green SJ, Swanson SR. Static constitutive relations for concrete. *Report No. AFWL-TR*-72-2, Air Force Weapons Laboratory, Kirkland Air Force Base, 1973.
5. WES. Concrete triaxial test data contained in Bažant ZP, Xiang Y, Adley MD, Prat PC, Akers SA. Microplane model for concrete, part II: data delocalization and verification. *ASCE Journal of Engineering Mechanics* 1996; **122**(3):255–262.
6. Burdette EG, Hilsdorf HK. Behaviour of laterally reinforced concrete columns. *Journal of the Structural Division ASCE* 1971; **97**:587–602.
7. MacGregor JG. *Reinforced Concrete: Mechanics and Design.* Prentice-Hall: Englewood Cliffs, NJ, 1988.
8. Nilson AH, Winter G. *Design of Concrete Structures.* McGraw-Hill: New York, 1979.
9. Park R, Paulay T. *Reinforced Concrete Structures.* Wiley: New York, 1975.
10. Kurt CE. Concrete filled structural plastic columns. *Journal of the Structural Division*, ASCE 1978; **104**(1):55–63.
11. Fardis NM, Khalili M. Concrete encased in fiberglass reinforced plastics. *ACI Journal* 1981; **78**(6):440–446.
12. Saadatmanesh H, Eshani MR, Li MW. Strength and ductility of concrete columns externally reinforced by fibre composites straps. *ACI Structural Journal* 1994; **91**(4):434–447.
13. Picher F, Rochette P, Labossiere P. Confinement of concrete cylinders with CFRP. In *Fibre Composites in Infrastructure* (*Proceedings, 1st International Conference, ICCI '96, Tucson*), Saadatmanesh H, Eshani MR (eds). University of Arizona: Tucson, 1996;829–841.

14. Kanatharana J, Lu L-W. Strength and ductility of concrete columns reinforced by FRP Tubes. In *Fibre Composites in Infrastructure (Proceedings, 2nd International Conference, ICCI '98, Tucson)*, Saadatmanesh H, Eshani MR (eds). University of Arizona: Tucson, 1998; 370–384.
15. Burgueno R, Davol A, Seible F. The carbon shell system for modular bridge components. In *Fibre Composites in Infrastructure (Proceedings, 2nd International Conference, ICCI '98. Tucson)* Saadatmanesh H, Eshani MR (eds). University of Arizona: Tucson, 1998; 341–354.
16. Bažant ZP, Bishop FC, Chang T-P. Confined compression tests of cement paste and concrete up to 330 ksi. *ACI Materials Journal* 1986; **33**:553–560.
17. Bažant ZP, Kim JJ, Brocca M. Finite strain tube-squash test for concrete at high pressures and shear angles up to 70°. *ACI Materials Journal* 1999; **96**(5):580–592.
18. Brocca M, Bažant ZP. Microplane model and metal plasticity. ASME *Applied Mechanics Reviews* 2000; **53**(10):265–281.
19. Taylor GI. Plastic strain in metals. *Journal of the Institute of Metals* 1938; **63**:307–324.
20. Batdorf SB, Budiansky B. A Mathematical theory of slip based on the concept of slip. *NACA Technical Notes* 1949; 1871.
21. Kröner E. Zur plastischen Verformung des Vielkristalls. *Acta Metallica* 1961; **9**:155–161.
22. Budiansky B, Wu TT. Theoretical prediction of plastic strains in polycrystals. *Proceedings of the 4th U.S. National Congress of Applied Mechanics* 1962; 1175–1185.
23. Lin TH, Ito M. Theoretical plastic distortion of a polycrystalline aggregate under combined and reversed stresses. *Journal of the Mechanics of Physics and Solids* 1965; **13**:103–115.
24. Hill R. Continuum micromechanics of elastoplastic polycrystals. *Journal of the Mechanics of Physics and Solids* 1965; **13**:89–102.
25. Hill R. Generalized constitutive relations for incremental deformation of metal crystals by multislip. *Journal of the Mechanics of Physics and Solids* 1966; **14**:95–102.
26. Rice JR. Inelastic constitutive relations for solids: an internal variable theory and its application to metal plasticity. *Journal of the Mechanics of Physics and Solids* 1971; **19**:433–455.
27. Zienkiewicz O, Pande G. Time-dependent multi-laminate model of rocks—A numerical study of deformation and failure of rock masses. *International Journal of Analytical and Numerical Methods in Geomechanics* 1977; **1**:219–247.
28. Pande G, Sharma K. Multilaminate model of clays—A numerical evaluation of the influence of rotation of principal axes. *ASCE Journal of Engineering and Mechanics* 1983; **109**(7):397–418.
29. Bažant ZP. Microplane model for strain controlled inelastic behavior. In *Mechanics of Engineering Materials*, Desai CS, Gallagher RH (eds), Chapter 3. Wiley: London, 1984; 45–59.
30. Bažant ZP. Oh BH. Microplane model for progressive fracture of concrete and rock. *ASCE Journal of Engineering Mechanics* **111**:559–582.
31. Bažant ZP, Prat PC. Microplane model for brittle plastic materials: I. Theory. *ASCE Journal of Engineering Mechanics* 1988; **114**(10):1672–1688.
32. Bažant ZP, Prat PC. Microplane model for brittle plastic materials: II. Verification. *ASCE Journal of Engineering Mechanics* 1988; **114**(10):1689–1702.
33. Bažant ZP, Adley MD, Carol I, Jirasek M, Akers SA, Rohani B, Cargile JD, Caner FC. Large-strain generalization of microplane model for concrete and applications. *ASCE Journal of Engineering Mechanics* 2001; **126**(9):971–980.
34. Bažant ZP, Caner FC, Adley MD, Akers SA. Fracturing of rate effect and creep in microplane model for dynamics. *ASCE Journal of Engineering Mechanics* 2001; **126**(9):962–970.
35. Bažant ZP, Caner FC, Carol I, Adley MD, Akers SA. Microplane model M4 for concrete: I Formulation with work-conjugate deviatoric stress. *ASCE Journal of Engineering Mechanics* 2001; **126**(9):954–961.
35a. Caner FC, Bažant ZP. Microplane model M4 for concrete II: Algorithm and calibration. *ASCE Journal of Engineering Mechanics* 2000; **129**(9):954–961.
36. Bažant ZP, Prat P. Creep of anisotropic clay: new microplane model. *ASCE Journal of Engineering Mechanics* 1987; **103**(7):1050–1064.
37. Prat P, Bažant ZP. Microplane model for triaxial deformation of soils. In *Numerical Models in Geomechanics (NUMOG III)*, Pietruszczak S, Pande G (eds). Elsevier: Niagara Falls, Canada, 1989; 139–146.
38. Prat P, Bažant ZP. Microplane model for triaxial deformation of saturated cohesive soils. *ASCE Journal of Geotechnical Engineering* 1991; **117**(6):891–912.
39. Prat P, Bažant ZP. A time dependent microplane model for creep of cohesive soils. In Mechanics Computing in the 90s and beyond. In *Proceedings of the ASCE-EMD Specialty Conference*, Adeli H, Sierakowski RL (eds). ASCE: Columbus, Ohio, USA 1991; 1224–1228.
40. Carol I, Bažant ZP. Damage and plasticity in microplane theory. *International Journal of Solids and Structures* 1997; **34**(29):3807–3835.
41. Bažant ZP, Xiang Y, Prat PC. Microplane model for concrete. I. Stress–strain boundaries and finite strain. *ASCE Journal of Engineering Mechanics* 1996; **122**(3):245–254. (With Errata vol. 123. p. 411).

42. Stroud AH. *Approximate Calculation of Multiple Integrals*. Prentice-Hall: Englewood Cliffs, N.J. 1971.
43. Bažant ZP, Oh BH. Efficient numerical integration on the surface of a sphere. *Zeitschrift für angerwandte Mathematik und Mechanik (ZAMM, Berlin)* 1986; **66**(1):37–49.
44. Doyle TC, Ericksen JL. Non-linear elasticity. *Advances in Applied Mechanics* 1956; **4**:53–115.
45. Ogden RW. *Non Linear Elastic Deformations*. Ellis Horwood and Wiley: Chichester, U.K. 1984.
46. Bažant ZP, Cedolin L. *Stability of Structures: Elastic, Inelastic, Fracture and Damage Theories*. Oxford University Press: New York, 1991.
47. Malvern LE. *Introduction to Mechanics of a Continuous Medium*. Prentice-Hall, Englewood Cliffs, NJ, 1969.
48. Rice JR. Mechanics of Solids. *Encyclopedia Britannica* (15th edn) vol. 23. (Encyclopedia Britannica Inc., Chicago) 1993; 737–747 and 773.
49. Flory TJ. Thermodynamic relations for high elastic materials. *Transactions, Faraday Society* 1961; **57**:829–838.
50. Sidoroff F. Un modèle viscoélastique non linéaire avec configuration intermédiaire. *Journal de Mécanique* 1974; **13**:679–713.
51. Simo JC. A framework for finite strain elastoplasticity based on maximum plastic dissipation and the multiplicative decomposition. *Computational Methods in Applied Mechanics and Engineering* 1988; **66**: 199–219, and **68**:1–31.
52. Bell JF. Contemporary perspectives in finite strain plasticity. *International Journal of Plasticity* 1985; **1**:3–27.
53. Lubliner J. Normality rules in large-deformation plasticity. *Mechanics of Materials* 1986; **5**:29–34.
54. Simo JC, Ortiz M. A unified approach to finite deformation elasto-plasticity based on the use of hyperelastic constitutive equations. *Computational Methods in Applied Mechanics and Engineering* 1985; **49**:177–208.
55. Bažant ZP. Finite strain generalization of small strain constitutive relations for any finite strain tensor and additive volumetric–deviatoric split. *International Journal of Solids and Structures* 1996; **33**:2887–2897 (special issue in memory of Juan Simo).
56. Bažant ZP. Recent advances in brittle-plastic compression failure: Damage localization, Scaling and finite strain. In *Computational plasticity: Fundamentals and Applications* (Proceedings of the 5th International Conference on Comput. Plasticity, COMPLAS 5, held in Barcelona), Owen DRJ, Oñate E, Hinton E (eds). International Centre for Numerical Methods in Engineering, Barcelona 1997; 3–19.
57. Hoger A. The stress conjugate to logarithmic strain. *International Journal of Solids and Structures* 1987; **23**(12):1645–1656.
58. Eterovic AL. Bathe KJ. A hyperelastic-based large-strain elastoplastic constitutive formulation. *International Journal for Numerical Methods in Engineering* 1990; **30**:1099–1114.
59. Gabriel G, Bathe KJ. Some computational issues in large strain elasto-plastic analysis. *Computers and Structures* 1995; **56**(2/3):249–267.
60. Hibbitt HD, Karlsson BI, Sorensen P. *ABAQUS Theory Manual, Version* 5.5. Hibbitt, Karlson and Sorensen, Inc.: Pawtucket, RI, 1994 (Section 4.6.1).

